Visfatin is upregulated in type-2 diabetic rats and targets renal cells

Young Sun Kang[1], Hye Kyoung Song[1], Mi Hwa Lee[1], Gang Jee Ko[1], Jee Young Han[2], Sang Youb Han[3], Kum Hyun Han[3], Hyoung Kyu Kim[4] and Dae Ryong Cha[1]

[1]Department of Internal Medicine, Korea University, Ansan City, Korea; [2]Department of Pathology, Inha University, Incheon, Korea; [3]Department of Internal Medicine, Inje University, Goyang City, Korea and [4]Department of Internal Medicine, Korea University, Seoul, Korea

Visfatin (also known as pre-B cell colony-enhancing factor) is a newly discovered adipocytokine that is preferentially produced by visceral fat and regulated by cytokines promoting insulin resistance. Here we determined its renal synthesis and physiology in a genetic model of type 2 diabetes in rats. These rats had higher levels of visfatin synthesis in both glomeruli and tubulointerstitium compared to control rats. Plasma visfatin levels were significantly increased in the early stages of diabetic nephropathy and positively correlated with body weight, fasting plasma glucose, and microalbuminuria. Interestingly, visfatin synthesis was found to occur in podocytes and proximal tubular cells, as well as in adipocytes *in vitro*. Further, in both renal cells, visfatin synthesis was significantly increased by high glucose in the media but not by angiotensin II. Additionally, visfatin treatment induced rapid uptake of glucose and was associated with increased translocation of GLUT-1 to the cellular membrane of both renal cell types. Furthermore, visfatin induced tyrosine phosphorylation of the insulin receptor, activated downstream insulin signaling pathways such as Erk-1, Akt, and p38 MAPK, and markedly increased the levels of TGFβ1, PAI-1, type I collagen, and MCP-1 in both renal cells. Thus, our results suggest that visfatin is produced by renal cells and has an important paracrine role in the pathogenesis of diabetic nephropathy.

Kidney International (2010) **78,** 170–181; doi:10.1038/ki.2010.98; published online 14 April 2010

KEYWORDS: diabetic nephropathy; glucose transporter-1; type-2 diabetic rats; visfatin

Correspondence: *Dae Ryong Cha, Department of Internal Medicine, Korea University Ansan-Hospital, 516 Kojan-Dong, Ansan City, Kyungki-Do 425-020, Korea. E-mail: cdragn@unitel.co.kr*

Received 29 June 2009; revised 8 January 2010; accepted 2 February 2010; published online 14 April 2010

Chronic kidney diseases (CKDs) are increasing to epidemic levels in the elderly and have been shown to be powerful cardiovascular risk factors.[1,2] Although a link between CKD and cardiovascular disease has been noted in with diabetes or non-diabetes patients,[3] the highest incidence of cardiovascular disease continues to be present in patients with both diabetes and CKD.[4] With respect to cardiovascular disease, the identity of numerous adipocytokines has emerged in obesity and metabolic syndrome research.[5,6] Indeed, there has been an evolving and intensive research effort on adipocytokines since the discovery of leptin in 1994.[7]

Visfatin is a newly discovered adipocytokine that appears to be preferentially produced by visceral fat.[8] Visfatin is identical to pre-B-cell colony-enhancing factor expressed in lymphocytes.[9] Expression of the pre-B-cell colony-enhancing factor is regulated by cytokines that promote insulin resistance such as lipopolysaccharide, interleukin-1, interleukin-6, and tumor necrosis factor-α.[10–12] A recent study contradicts several previously published reports on visfatin. This study failed to confirm original results from human diabetic patients.[13] Several subsequent reports have provided evidence that visfatin is not an actual adipocytokine, but rather a novel marker of inflammation. Visfatin expression is increased in foam cell macrophages that have a role in plaque destabilization within unstable atherosclerotic regions.[14] Plasma visfatin concentrations are related to endothelial dysfunction in type-2 diabetic patients and patients with CKD.[15,16] In addition, visfatin expression is detected in synovial fibroblasts in patients with rheumatoid arthritis, and visfatin itself activates nuclear factor-κB and various related pro-inflammatory cytokines in cultured synovial fibroblasts.[17] Collectively, these results suggest a new physiological role of visfatin in organ injury.

We have previously observed that visfatin synthesis is increased by high glucose stimulus in mesangial cells, and also that visfatin may contribute to increased glucose influx in mesangial cells, thereby accelerating diabetic nephropathy through aggravation of metabolic alterations.[18] In this study, we investigated whether visfatin synthesis is increased in the diabetic kidney in type-2 diabetic rats, and evaluated their association with several biochemical parameters.

Additionally, to define the molecular mechanism of visfatin, we evaluated the effect of high glucose on visfatin synthesis and the effect of visfatin on glucose metabolism in both podocytes and proximal tubular cells (PTCs). Finally, we evaluated the direct effect of visfatin on the synthesis of pro-inflammatory and pro-fibrotic cytokines synthesis in cultured podocytes and PTCs.

RESULTS

Biochemical parameters in experimental animals

Table 1 shows the various biochemical results obtained for each experimental group of animals. Fasting plasma glucose levels were significantly higher in Otsuka Long-Evans Tokushima Fatty (OLETF) rats (143.6 ± 17 mg/dl) than Long-Evans-Tokushima-Fatty (LETO) rats (108.0 ± 10 mg/dl; $P = 0.026$). Kidney/body weight was also significantly higher in OLETF rats as compared with in LETO rats. There were no significant differences in serum creatinine concentrations and urine volume between the two groups. Systolic blood pressure, measured at the end of the study period, was greater in OLETF rats than in LETO rats. Urinary albumin excretion in OLETF rats was significantly higher than in the LETO rats at 20 weeks of age, and this difference was further increased at the end of the study period. OLETF rats exhibited marked glucose intolerance compared with LETO, which was confirmed by an intraperitoneal glucose tolerance test (GTT). In accordance with glucose intolerance, OLETF rats showed significantly higher levels of plasma cholesterol and triglyceride levels (cholesterol, LETO: 103 ± 5.4, OLETF: 141 ± 32, $P = 0.027$; triglyceride, LETO: 43 ± 9, OLETF: 184 ± 24, $P = 0.003$). Although plasma adiponectin levels were not significantly different between the two groups, plasma insulin levels were significantly higher in OLETF rats than in LETO rats (LETO: 1.02 ± 0.14, OLETF: 2.54 ± 0.25, $P = 0.005$). In addition, homeostasis model assessment (HOMA) insulin resistance indexes (HOMA-IRs) also showed significantly higher levels in OLETF rats as compared with that in LETO rats (LETO: 0.43 ± 0.11, OLETF: 0.63 ± 0.06, $P = 0.047$). To examine the role of visfatin in diabetic nephropathy, we measured the plasma concentrations of visfatin at different time points in the experimental rats. Visfatin levels were significantly elevated in OLETF rats as compared with LETO rats at 20 weeks, which was during the early stages of diabetic nephropathy, and this trend continued until the end of the study period (Table 1). Interestingly, plasma visfatin levels were positively correlated with body weight, microalbuminuria, fasting plasma glucose levels, and HOMA-IRs (Table 2).

Histopathological changes in experimental animals

Figure 1 shows representative renal pathology changes in the experimental groups at the end of the study period. According to a semi-quantitative scoring system, OLETF rats showed more severe glomerulosclerosis than LETO rats (Figure 1a and b); however, there were no remarkable findings of tubulo-interstitial fibrosis even in OLETF rats, which indicates that the differences were not significant. We

Table 2 | Correlation analysis between plasma visfatin levels and biochemical parameters in experimental animals

Parameters	*r*-value	*P*-value
Body weight	0.424	0.027
Microalbuminuria	0.317	0.031
Plasma creatinine	0.239	0.573
Systolic blood pressure	0.213	0.423
Fasting plasma glucose	0.551	0.021
Plasma insulin	0.243	0.231
Plasma adiponectin	0.263	0.371
HOMA-IR	0.351	0.044

Abbreviation: HOMA-IR, the homeostasis model assessment index.
Correlation analysis was performed using Spearman rank correlations.

Table 1 | Biochemical parameters in experimental animals

	LETO (20 weeks)	OLETF (20 weeks)	LETO (50 weeks)	OLETF (50 weeks)	*P*-value
Body weight (g)	316.6 ± 32.5	472.3 ± 31.2*	492.1 ± 47.2	619.3 ± 32.2*	0.025
Kidney/BW $\times 10^{-3}$	NA	NA	0.29 ± 0.04	0.32 ± 0.10*	0.036
FPG (mg/dl)	112 ± 12.1	131.4 ± 15.2*	108.0 ± 10.0	143.6 ± 17.0*	0.026
P-Cr (mg/dl)	0.54 ± 0.12	0.55 ± 0.25	0.67 ± 0.05	0.58 ± 0.13	
UV (ml/day)	12.5 ± 10.5	16.1 ± 14.3	18.6 ± 11.3	14.1 ± 1.73	
UAE (μg/mgCr/day)	42.36 ± 11.52	84.3 ± 11.5*	34.72 ± 1.44	159.7 ± 51.14#	<0.001
SBP (mm Hg)	NA	NA	128.5 ± 20.6	147.2 ± 18.1**	0.008
P-visfatin (pg/ml)	62.4 ± 13.7	103.4 ± 21.6*	68.3 ± 46	108.5 ± 19.4*	0.035
Cholesterol (mg/dl)	NA	NA	103.0 ± 5.4	141.0 ± 32.0*	0.027
Triglyceride (mg/dl)	NA	NA	43.0 ± 9.01	184.0 ± 24.0**	0.003
P-insulin (ng/ml)	NA	NA	1.02 ± 0.14	2.54 ± 0.25**	0.005
HOMA-IR	NA	NA	0.43 ± 0.11	0.63 ± 0.06*	0.047
GTT (basal) (mg/dl)	NA	NA	113.4 ± 12.5	131.2 ± 17.6	
GTT (30 min) (mg/dl)	NA	NA	201.5 ± 22.4	465.2 ± 37.0#	<0.001
GTT (60 min) (mg/dl)	NA	NA	188.3 ± 27.6	410.0 ± 41.2#	<0.001
GTT (90 min) (mg/dl)	NA	NA	151.5 ± 19.6	355.7 ± 16.6#	<0.001
GTT (120 min) (mg/dl)	NA	NA	116.9 ± 10.7	298.6 ± 15.2**	0.009

Abbreviations: BW, body weight; FPG, fasting plasma glucose; GTT, glucose tolerance test; HOMA-IR, the homeostasis model assessment index; NA, not available; P-Cr, plasma creatinine concentration; P-visfatin, plasma visfatin concentration; SBP, systolic blood pressure; UAE, urinary albumin excretion; UV, urine volume.
The values are expressed as the mean ± s.e.m. Statistical analyses were performed between LETO and OLETF groups at the same time periods. *$P < 0.05$, LETO versus OLETF; **$P < 0.01$, LETO versus OLETF; #$P < 0.001$, LETO versus OLETF (number of replicates for measurement; duplicates for P-Cr, UAE, P-visfatin, and lipid profile; n=10 for SBP measurement).

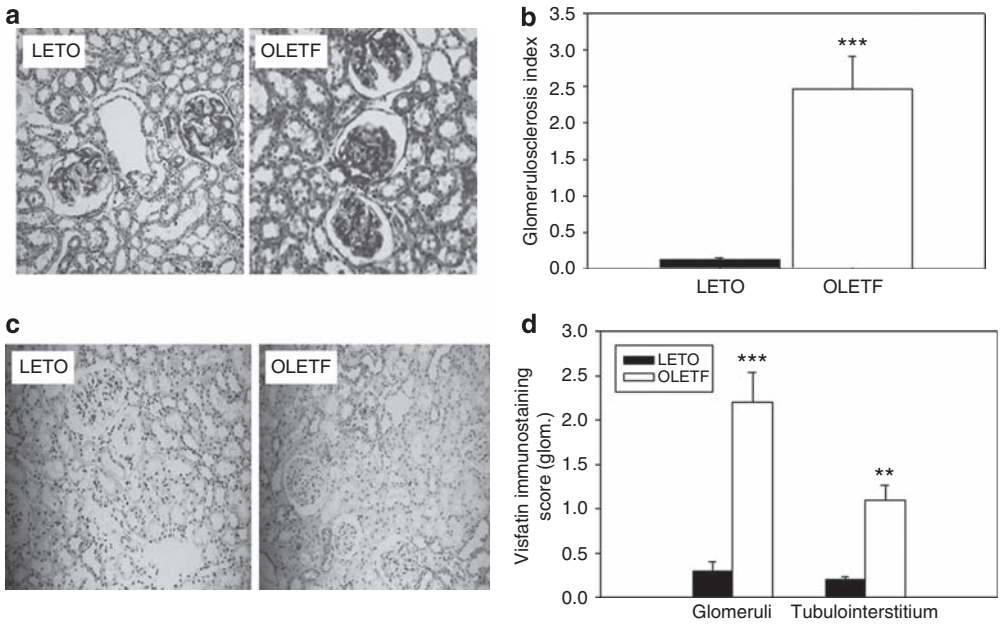

Figure 1 | Representative renal histology and immunohistochemistry for visfatin in experimental animals. (**a**) Periodic acid–Schiff staining. (**b**) Glomerulosclerosis index. (**c**) Immunostaining for visfatin. (**d**) Immunostaining score for visfatin. Data are shown as the mean ± s.e.m. Original magnification ×200. More than 50 and 60 glomeruli, and 10 randomly selected tubulointerstitial fields were evaluated; $^{**}P = 0.007$, LETO versus OLETF; $^{***}P < 0.001$, LETO versus OLETF.

performed visfatin immunostaining and found that OLETF rats exhibited markedly increased immunoreactivity in both glomeruli and tubulo-interstitium when compared with LETO rats. In addition, visfatin immunoreactivity was primarily increased in the mesangium, podocytes, and proximal tubular epithelium (Figure 1c and d, Supplementary Figure S1).

Effect of high glucose and angiotensin II on visfatin production in cultured podocytes and PTCs

To confirm the synthesis of visfatin in podocytes and murine cortical tubule (MCT) cells, reverse transcription–PCR was performed. We used 3T3-L1 adipocytes as positive controls due to their high expression of visfatin. As shown in Figure 2a, visfatin was also expressed in podocytes and MCT cells as well as adipocytes. The effect of high glucose and angiotensin II on visfatin synthesis was subsequently examined. Visfatin gene expression and protein synthesis were increased significantly after high glucose stimulation in both podocyes and MCT cells; however, angiotensin II stimulation did not induce any changes in visfatin production (Figure 2b–f, Supplementary Figure S2).

Effect of visfatin on 2-DOG uptake in podocytes and PTCs

To examine the biological effect of visfatin, we investigated 2-deoxyglucose uptake after visfatin stimulation in renal cells using a 2-deoxy-D-glucose (2-DOG) uptake assay. First, a time course of 2-DOG uptake after treatment with 100 ng/ml of visfatin was performed. As shown in Figure 3, visfatin treatment induced rapid uptake of 2-DOG in both podocytes and MCT cells, with maximal stimulation at 20 min followed by rapid decrease to control levels at 30 min. As expected, insulin treatment induced rapid uptake of 2-DOG in renal cells that peaked at 20 min. Cytochalasin-B, an endocytosis inhibitor including glucose transporter, completely abolished visfatin-stimulated glucose uptake to basal levels, showing that visfatin-induced glucose uptake was mediated by glucose transporters (Figure 3a and b). Furthermore, stimulation of 2-DOG uptake by visfatin in MCT cells increased in a dose-dependent manner beginning with a concentration of 10 ng/ml and reaching maximal stimulation at 100 ng/ml. Conversely, there was no dose-dependent effect of visfatin-induced glucose uptake in podocytes (Figure 3c and d).

Effect of visfatin on GLUT-1 synthesis and translocation in podocytes and PTCs

Next, we investigated the ability of a glucose transporter to mediate visfatin-induced glucose transport. Among the facilitative glucose transporters, glucose transporter-1 (GLUT-1) has been shown to be the major glucose transporter in renal cells, and thus the possibility that visfatin stimulation increases the expression of GLUT-1 was examined. As shown in Figure 4, visfatin treatment induced a significant increase in the mRNA expression of GLUT-1 in both podocytes and MCT cells (Figure 4a and b). To further confirm the translocation of GLUT-1 to the cellular membrane, western blotting using the membrane fraction of the cells was performed (Supplementary Figure S3). As shown in Figure 4, GLUT-1 expression was increased in the plasma membrane of cells after visfatin stimulation. As positive control, GLUT-1 translocation into the cell membrane induced by insulin stimulation was also observed (Figure 4c and d).

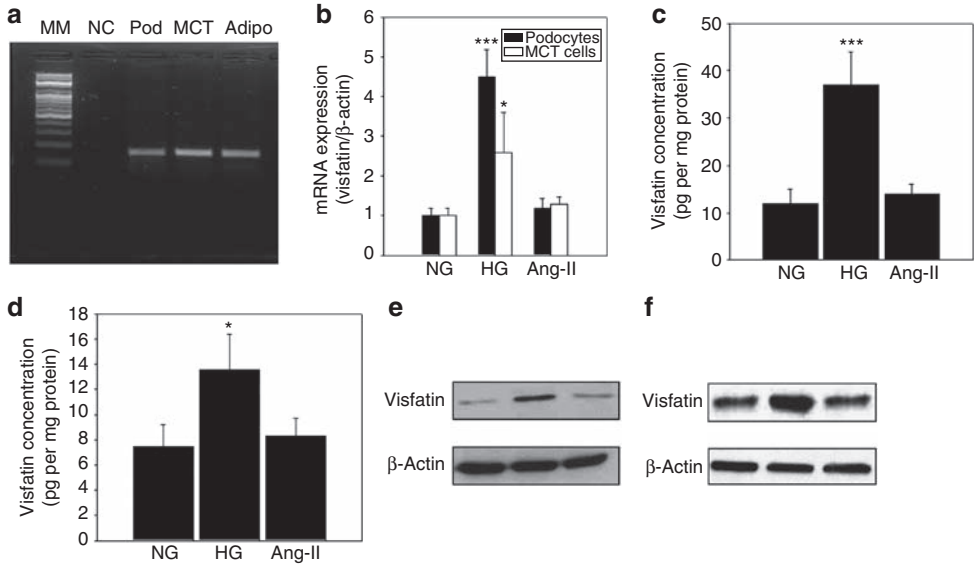

Figure 2 | Synthesis of visfatin and the effect of high glucose and angiotensin II on visfatin production in experimental cells. (**a**) PCR results for visfatin in cultured cells. A representative reverse transcription-PCR showing a 143-bp product. As positive control, 3T3-L1 adipocytes were used. (**b**) Effect of high glucose and angiotensin II on visfatin mRNA expression in cultured cells. Effect of high glucose and angiotensin II on visfatin protein secretion in cultured podocytes (**c**) and MCT cells (**d**). A representative western blot for visfatin in cultured podocytes (**e**) and MCT cells (**f**). Secretory visfatin protein levels were measured by ELISA. Cells were exposed to a high-glucose medium (30 mM of D-glucose) or angiotensin II (100 nM) for 48 h. The data are shown as the mean ± s.e.m. Adipo, 3T3L1 adipocytes; Ang-II, angiotensin II; HG, high glucose; MCT, MCT cells; MM, 100-bp molecular weight marker; NC, negative control; NG, normal glucose; Pod, podocytes. *$P = 0.031$ versus NG; ***$P < 0.001$ versus NG ; $n = 6$ in each condition.

Effect of visfatin on insulin signal transduction

We next examined whether visfatin-induced glucose uptake occurs through insulin signaling pathway. First we observed the effect of visfatin on the tyrosine phosphorylation of the insulin receptor (IR). As shown in Figure 5, visfatin stimulation induced tyrosine phosphorylation of IR and IR substrate-1 (IRS-1), and binding of p85 to IRS-1 molecule in both podocytes and MCT cells.

Effect of visfatin on Akt, Erk-1/2, p38 MAPK activation, and pro-fibrotic molecule synthesis

As visfatin was found to increase glucose transport and induce the tyrosine phosphorylation of the IR, we next examined the effect of visfatin on Akt, extracellular signal-regulated kinase-1 (Erk-1)/2, and p38 mitogen-activated protein kinase (MAPK) activation, all of which are important downstream components of the insulin signaling pathway. As shown in Figure 6, activation of Akt and Erk-1/2, as assessed by measuring the levels of phospho-specific Akt and Erk-1/2, was found to rapidly increase in response to visfatin after 1 min, and then gradually decreased. Likewise, activation of p38 MAPK was found to increase after 5 min, with maximal activity occurring at 30 min followed by gradual decrease, although to levels that remained higher than that in the controls. By contrast, total Akt, Erk-1/2, and p38 MAPK protein levels did not differ among the various treatment groups.

Because visfatin increased glucose uptake and activated the downstream components of the insulin signaling pathway, we examined the effect of augmented glucose influx induced by visfatin on changes in the synthesis of pro-inflammatory and pro-fibrotic molecules such as transforming growth factor-β1 (TGFβ1), plasminogen activator inhbitor-1 (PAI-1), monocyte chemoattractant peptide-1 (MCP-1), and collagen. As shown in Figure 6, visfatin stimulation significantly increased the gene expression of TGFβ1, PAI-1, MCP-1, and type-I collagen in both podocytes and MCT cells. Prior treatment with cytochalasin-B completely abolished visfatin-induced TGFβ1, PAI-1, MCP-1, and type-I collagen gene expression, which implied that the overexpression of these targets induced by visfatin occurred through an augmented glucose influx into cells. To further confirm the effect of visfatin on MCP-1, PAI-1, and collagen protein synthesis, ELISA and western blot analysis were performed. As shown in Figure 7, MCP-1, PAI-1, and collagen protein secretion was markedly increased by visfatin treatment, which was completely abolished by treatment with cytochalasin-B. As visfatin induced activation of MAPK, we further examined whether pharmacological inhibitors of MAPK inhibit visfatin-induced glucose uptake. As shown in Figure 8, blockade of the MAPK pathway did not inhibit visfatin-induced glucose uptake in both cells.

DISCUSSION

In this study, we found that visfatin was synthesized in both renal cells and adipocytes, and that plasma visfatin concentrations were significantly increased during the early stages of diabetic nephropathy in type-2 diabetic rats.

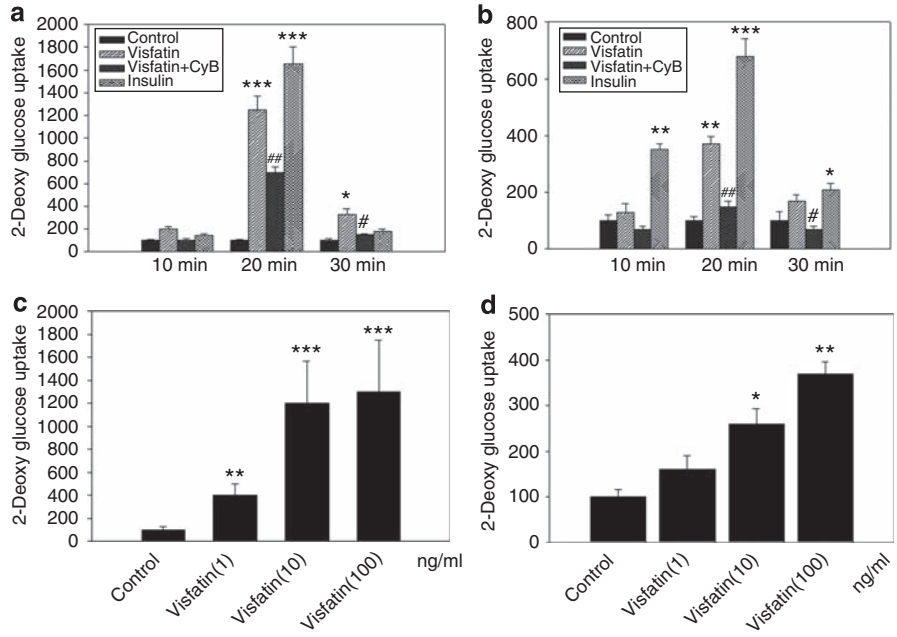

Figure 3 | Effect of visfatin on 2-DOG uptake in experimental cells. (**a**) 2-DOG uptake in podocytes. (**b**) 2-DOG uptake in MCT cells. Experimental cells were treated in the presence or absence of 100 ng/ml of visfatin at the indicated time intervals. In some wells, 10 μM of cytochalasin-B, an inhibitor of glucose transporters, was pretreated for 30 min before visfatin treatment. As positive control, 100 nM of insulin was used. Radioactivity was normalized for total protein concentration in each condition and 2-DOG uptake was expressed as a % change compared with controls. The dose-dependent effect of visfatin on 2-DOG uptake in podocytes (**c**) and MCT cells (**d**). Because peak glucose uptake occurred at 20 min, cells were treated with different concentrations of visfatin at final concentrations of 1, 10, or 100 ng/ml for 20 min, and glucose uptake was measured. The data are shown the mean ± s.e.m. CyB, cytochalasin-B. (**a**): $^{*}P = 0.041$ and $^{***}P < 0.001$ versus control; $^{\#}P = 0.032$ and $^{\#\#}P = 0.007$ versus visfatin; (**b**): $^{*}P = 0.026$ and $^{**}P = 0.003$ and $^{***}P < 0.001$ versus control; $^{\#}P = 0.041$ and $^{\#\#}P = 0.003$ versus visfatin; (**c**): $^{**}P = 0.005$ and $^{***}P < 0.001$ versus control; (**d**): $^{*}P = 0.035$ and $^{**}P < 0.006$ versus control; $n = 6$ in each condition.

Visfatin expression was markedly upregulated in the diabetic kidney both in the glomeruli and proximal tubules. In addition, stimulation with high glucose, but not angiotensin II, markedly upregulated visfatin synthesis in both glomerular podocytes and PTCs. Interestingly, visfatin-stimulated glucose uptake in glomerular podocytes and PTCs was mediated by GLUT-1. Furthermore, administration of exogenous visfatin induced increased synthesis of pro-fibrotic and pro-inflammatory molecules, including TGFβ1, PAI-1, MCP-1, and type-I collagen. Together, these results suggest that endogenous visfatin produced by podocytes and PTCs can stimulate glucose uptake and is followed by accelerated glucose-mediated metabolic abnormalities in the diabetic kidney.

Adipose tissue is now believed to be an endocrine organ, and within this tissue, the visfatin gene in humans is known to be expressed predominantly in the visceral layer rather than in the subcutaneous layer.[19] Adipocytokines, which are secreted by adipose tissue, have been studied for their association with insulin resistance and metabolic syndrome, including glucose intolerance and hyperlipidemia. Visfatin binds directly to the IR at a site distinct from insulin, where it exerts a hypoglycemic effect by reducing glucose release from hepatocytes and stimulating glucose utilization in peripheral tissue.[20] Recent clinical studies have shown that plasma levels of visfatin are increased in obese and type-2 diabetic patients, and are related to insulin resistance.[8,21]

The results of several studies have begun to elucidate the role of visfatin as an adipocytokine in obesity, metabolic syndrome, and cardiovascular disease. Conversely, there is some doubt as to whether visfatin is an actual adipocytokine.[22] Other studies have reported that visfatin is distributed ubiquitously in all tissues and exists primarily in the cell nucleus and cytoplasm.[23,24] Furthermore, these studies also showed that visfatin is secreted during adipocyte differentiation and cell lysis in a cell-cycle-dependent manner.[23,24] Therefore, the role of visfatin as a secreted protein should be interpreted with caution. Thus, elucidation of the potential role for visfatin remains an attractive research target, given its already-described insulin-mimicking biological and physiological effects.

However, recent studies have also provided evidence that visfatin has pro-inflammatory properties and that its expression is increased in inflammatory conditions such as acute lung injury, sepsis, and rheumatoid arthritis.[10,17,25] In addition, plasma visfatin concentrations have been correlated with endothelial dysfunction in type-2 diabetic patients and patients with CKD.[15,16] Furthermore, several studies have failed to identify an association between circulating levels of visfatin and insulin sensitivity.[26–29] Collectively, these results suggest a new physiological role of visfatin in organ injury.

To the best of our knowledge, this is the first report to show that visfatin is synthesized in the kidney and that its

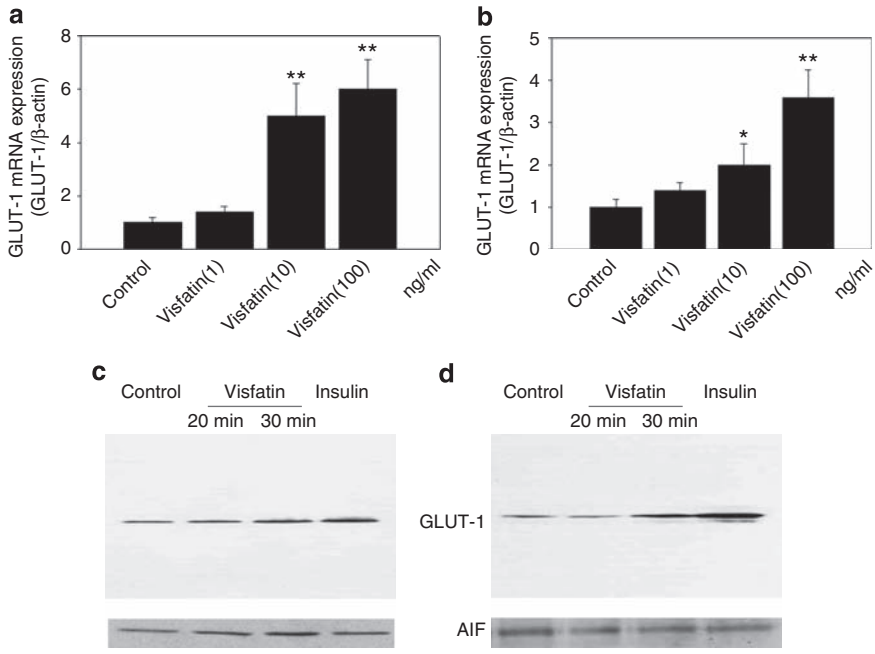

Figure 4 | Effect of visfatin on GLUT-1 synthesis and localization in experimental cells. Effect of visfatin on GLUT-1 gene expression in podocytes (**a**) and MCT cells (**b**). Cells were treated with different concentrations of visfatin at final concentrations of 1, 10, or 100 ng/ml, and harvested for extraction of total RNA. A representative western blot showing the effect of visfatin on the expression of GLUT-1 protein in cellular membranes in podocytes (**c**) and MCT cells (**d**). Cytosol and membrane fractions were prepared using the Qproteom Cell Compartment kit, and 50 μg of each protein sample was loaded for electrophoresis on a 10% SDS–polyacrylamide gel. GLUT-1 protein was detected as a single band of approximately 55 kDa. To confirm equal loading and microsomal fractionation, a western blotting was performed for AIF. The data are shown as the mean ± s.e.m. GLUT-1, glucose transporter-1; (**a**): $^{**}P = 0.007$ for visfatin 10 and $^{**}P = 0.003$ for visfatin 100 versus control; (**b**): $^{*}P = 0.047$ and $^{**}P = 0.005$ versus control; $n = 6$ in each condition. AIF, apoptosis-inducing factor.

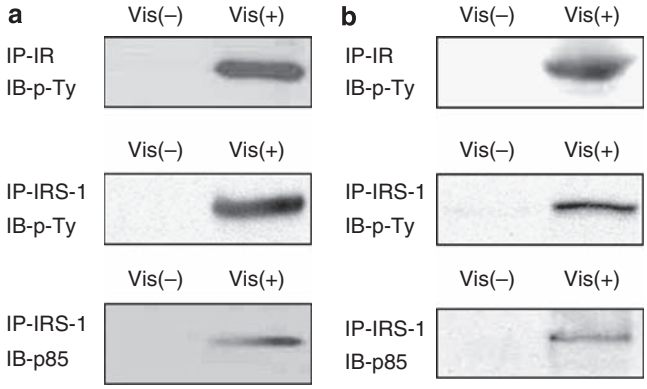

Figure 5 | Effect of visfatin on insulin signal transduction. Tyrosine phosphorylation of IR and IRS-1 and binding of p85 to IRS-1 was determined in cultured podocytes (**a**) and MCT cells (**b**). Cells were cultivated in the presence or absence of 100 ng/ml of visfatin. For measurement of tyrosine phosphorylation of the IR and IRS-1, and binding of p85 to IRS-1, cellular protein extract was analyzed by immunoprecipitation using antibody to the IR and IRS-1, and detected by immunoblotting using antibody to phosphotyrosine or antibody to p85. IB, immunoblotting; IP, immunoprecipitation; IR, insulin receptor; IRS-1, insulin receptor substrate-1; p-Ty, phosphotyrosine.

synthesis is upregulated in the diabetic kidney. In this study, we used OLETF rats, which are a genetic model of type-2 diabetes mellitus and are characterized by insulin resistance and obesity.[30] These characteristics make this model appropriate for a type-2 diabetic animal model. The insulin resistance status of OLETF rats was clearly shown by GTT, which showed that plasma levels of insulin and HOMA-IR were significantly increased, and that these changes were accompanied by lipid abnormalities. Interestingly, plasma levels of visfatin were significantly increased in type-2 diabetic rats, which is consistent with a report by Chen *et al.*,[21] which shows that plasma visfatin concentrations are elevated in type-2 diabetic patients.

In this study, we found that plasma visfatin concentrations were elevated during the early stages of diabetic nephropathy and were correlated with body weight, microalbuminuria, fasting plasma glucose, and HOMA-IR. Although it was not clear whether the early increase in plasma visfatin levels in diabetic rats had a causative role in tissue injury as a pro-inflammatory molecule or whether it was a compensatory response to decrease insulin resistance, the association with microalbuminuria was interesting. These results support the possibility that in addition to obesity and metabolic syndrome, visfatin may be associated with diabetic nephropathy and/or have a role as an early marker of diabetic nephropathy through microalbuminuria.

Hyperglycemia in diabetes is associated with increased glucose uptake into cells, which leads to cellular metabolic alterations that have long been considered an important pathophysiological mechanism for diabetic microvascular complications.[31,32] There are many studies suggesting that

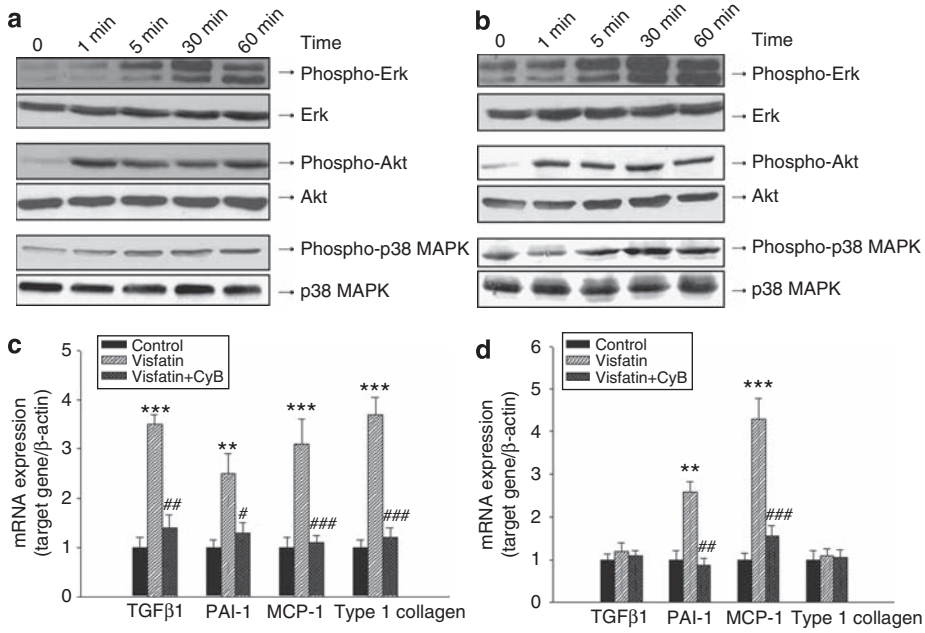

Figure 6 | Effect of visfatin on Akt, Erk-1/2, and p38 MAPK activation and pro-fibrotic molecule synthesis in experimental cells. A representative western blot of phospho-specific Akt, phospho-specific Erk-1/2, and phospho-specific p38 MAPK in response to visfatin treatment at the indicated time points in podocytes (**a**) and MCT cells (**b**). Effect of visfatin on mRNA expression of TGFβ1, PAI-1, MCP-1 and type-I collagen synthesis in podocytes (**c**) and MCT cells (**d**). Cells were exposed to visfatin (100 ng/ml) for 48 h and harvested for extraction of total RNA. In some wells, cells were pretreated for 30 min with 10 μM of cytochalasin-B. The data are shown as the mean ± s.e.m. CyB, cytochalasin-B; MCP-1, monocyte chemoattractant peptide-1; PAI-1, plasminogen activator inhbitor-1; TGFβ1, transforming growth factor-β1. (**c**): $^{**}P = 0.004$ and $^{***}P < 0.001$ versus control; $^{\#}P = 0.039$, $^{\#\#}P = 0.008$ and $^{\#\#\#}P < 0.001$ versus visfatin; (**d**): $^{**}P = 0.005$ and $^{***}P < 0.001$ versus control; $^{\#\#}P = 0.009$, and $^{\#\#\#}P < 0.001$ versus visfatin; $n = 6$ in each condition.

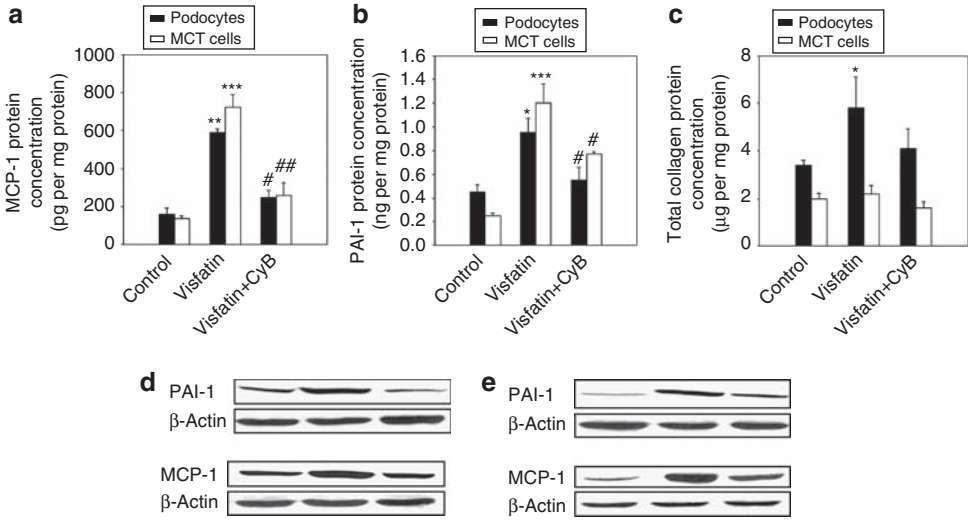

Figure 7 | Effect of visfatin on profibrotic protein synthesis in experimental cells. Effect of visfatin on MCP-1 (**a**), PAI-1 (**b**), and collagen (**c**) protein secretion in experimental cells. A representative western blot for PAI-1 and MCP-1 in cultured podocytes (**d**) and MCT cells (**e**). Levels of secreted PAI-1, MCP-1, and collagen protein were measured by ELISA. Each protein concentration was corrected for total cellular protein content. Cells were exposed to visfatin (100 ng/ml) for 48 h and harvested for extraction of protein. In some wells, cells were pretreated for 30 min with 10 μM of cytochalasin-B. The data are shown are the mean ± s.e.m. CyB, cytochalasin-B; MCP-1, monocyte chemoattractant peptide-1; PAI-1, plasminogen activator inhbitor-1. (**a**): $^{**}P = 0.004$ and $^{***}P < 0.001$ versus control; $^{\#}P = 0.012$ and $^{\#\#}P = 0.009$ versus visfatin; (**b**): $^{*}P = 0.012$ and $^{***}P < 0.001$ versus control; $^{\#}P = 0.040$ vs. visfatin; (**c**): $^{*}P = 0.045$ versus control; $n = 6$ in each condition.

increased glucose uptake by MCs induces the accumulation of mesangial extracellular matrix protein, which is a pathological feature of diabetic nephropathy.[33,34] Although there is not sufficient evidence to indicate that increased glucose uptake in podocytes and PTCs could induce direct metabolic alterations in these cells, it is generally considered

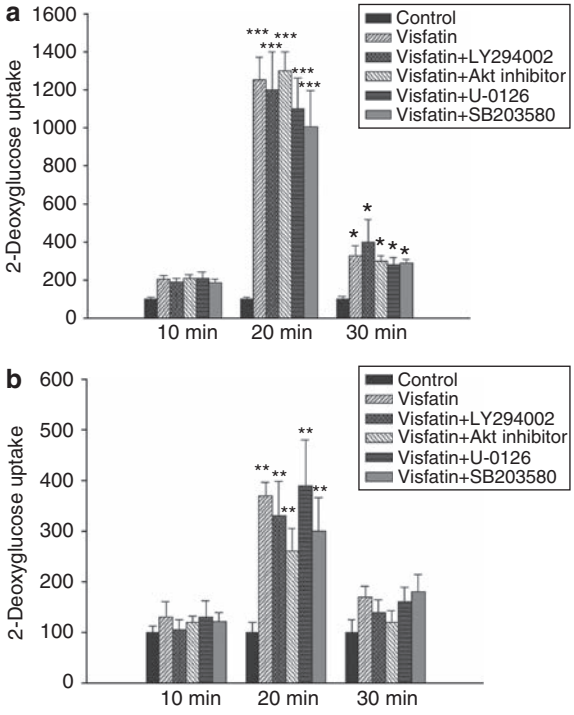

Figure 8 | Effect of MAPK inhibitors on glucose uptake in experimental cells. Effect of MAPK inhibitors on glucose uptake in cultured podocytes (**a**) and MCT cells (**b**). Experimental cells were pretreated with LY294002 (PI3K inhibitor, 1 μM), Akt inhibitor (10 μM), U-0126 (Erk inhibitor, 40 μM), and SB 203580 (p38 MAPK inhibitor, 10 μM) for 30 min before being incubated with visfatin (100 ng/ml) for 30 min. 2-DOG uptake was determined at the indicated time intervals. (**a**): $^{*}P = 0.041$ for visfatin; $P = 0.042$ for visfatin + LY294002; $P = 0.044$ for visfatin + Akt inhibitor; $P = 0.048$ for visfatin + U-0126; $P = 0.043$ for visfatin + SB 203580; and $^{***}P < 0.001$ versus control. (**b**): $^{**}P = 0.003$ for visfatin; $P = 0.006$ for visfatin + LY294002; $P = 0.009$ for visfatin + Akt inhibitor; $P = 0.004$ for visfatin + U-0126; and $P = 0.008$; $n = 6$ in each condition.

that increased glucose uptake is the primary pathological mechanism for diabetic tissue injury.

In this study, high-glucose stimulation was found to significantly increase the synthesis of visfatin; however, angiotensin II, another important mediator of diabetic nephropathy, did not similarly induce upregulation of visfatin synthesis. This result is in agreement with a recent report showing that infusion of exogenous glucose increases plasma visfatin levels in a healthy population.[35] These results suggest the possibility that a high-glucose condition in a diabetic environment could continuously stimulate visfatin synthesis from podocytes and PTCs *in vivo*.

We also observed that treatment with visfatin rapidly stimulated 2-DOG uptake in podocytes and PTCs. In addition, the visfatin-induced increase in 2-DOG uptake could be abolished by the addition of cytochalasin-B in visfatin-treated cells, suggesting that 2-DOG uptake occurred primarily through facilitative glucose transporters. However, cytochalasin-B is not a specific inhibitor of glucose transporters but an endocytosis inhibitor that blocks several cellular functions. It may be possible that inhibition of endocytosis mediated by cytochalasin-B may affect cellular function independent of effects of decreased glucose uptake into cells. In line with this observation, we found that expression of GLUT-1, which is a constitutional glucose transporter and is present at the plasma membrane of most cells,[36,37] was significantly increased after visfatin treatment. In addition, we observed that treatment with visfatin resulted in the translocation of GLUT-1 in both podocytes and PTCs. This translocation was observed after 10 min of visfatin stimulation and peaked at 20 min of stimulation. These results were in agreement with the 2-DOG uptake results, which showed maximal uptake after 20 min of visfatin stimulation. Western blot analysis using the membrane fraction of cells clearly showed translocation of GLUT-1 after visfatin stimulation.

We also studied whether the downstream signaling molecules induced by glucose uptake in cells were activated in response to visfatin treatment. We observed that visfatin treatment induced the tyrosine phosphorylation of the IR and IRS-1, and binding of p85 to IRS-1 molecule in both podocytes and PTCs. Interestingly, we found that protein kinase-B, which is an important downstream target of phosphoinositide-3-kinase and has an important role in glucose metabolism, was activated by visfatin treatment. We also observed that visfatin was able to activate Erk-1/2 and p38 MAPK, both of which are important regulators of cell proliferation and extracellular matrix synthesis. This result suggested that visfatin treatment activated IR signaling pathway and induced glucose uptake, which was followed by activation of Akt, Erk-1/2, and p38 MAPK, all of which are downstream signaling molecules of cellular glucose influx.

Another important finding in this study was that exogenous visfatin treatment increased the synthesis of pro-fibrotic and pro-inflammatory molecules such as TGFβ1, PAI-1, MCP-1, and type-I collagen. The visfatin-induced increase in these molecules could be abrogated by cytochalasin-B treatment, suggesting that visfatin-induced TGFβ1, PAI-1, MCP-1, and type-I collagen synthesis was mediated by cellular glucose uptake. On the basis of these observations, we hypothesized that increased visfatin production under high-glucose conditions induced an increase in endogenous visfatin synthesis from renal cells, and consequently, visfatin could stimulate glucose uptake to accelerate metabolic alterations, including overproduction of pro-fibrotic molecules. The interaction between visfatin and GLUT-1 shown in this study may elucidate a new physiological role of visfatin in the pathogenetic mechanism of diabetic nephropathy. These results are in agreement with recent reports that circulating levels of visfatin are associated with endothelial dysfunction in patients with CKD and that visfatin itself activates various pro-inflammatory cytokines in cultured synovial fibroblasts.[15–17]

In conclusion, the results of this study suggest a new physiological role of visfatin in diabetic nephropathy. Visfatin synthesis was markedly increased in diabetic glomeruli and tubules in type-2 diabetic rats. Plasma visfatin concentrations

were significantly elevated in the early stages of diabetic nephropathy. On the basis of these results, we hypothesize that increased visfatin synthesis from renal cells under high-glucose conditions possibly contributes to increased glucose influx into cells through GLUT1, thereby accelerating diabetic nephropathy through aggravation of metabolic alterations. Thus, visfatin may have an important role in the pathogenesis of diabetic nephropathy. More *in vivo* studies are necessary to define the role of visfatin in the pathogenesis of diabetic nephropathy.

METHODS

Animal studies

OLETF rats were supplied by the Tokushima Research Institute (Otsuka Pharmaceutical Co., Tokyo, Japan) and were used as a type-2 diabetic model. Age-matched male LETO rats served as the genetic control for OLETF rats. Rats at 16 weeks of age had free access to rat food and tap water, and were caged individually under a controlled temperature ($23 \pm 2\,^{\circ}C$) and humidity ($55 \pm 5\%$) environment with an artificial light cycle. At the end of the study period, systolic blood pressure was measured by tail-cuff plethysmography (LE 5001-Pressure Meter; Letica SA, Barcelona, Spain). Plasma glucose levels were measured by a glucose oxidase-based method and creatinine levels were determined by a modified Jaffe method. Plasma insulin levels and plasma adiponectin levels were measured using an ELISA kit (Linco Research, St Charles, MO, USA). The HOMA-IR was calculated using the following formula: fasting glucose (mmol/l) $\times$ fasting insulin (mU/l)/22.5. Plasma triglyceride and cholesterol analyses were performed using a GPO-Trinder kit (Sigma, St Louis, MO, USA). A GTT was performed to assess the insulin resistance status of each group. GTTs were performed after an 8-h fasting period and blood samples were collected through the tail vein. Rats received 2 g dextrose/kg body weight by intraperitoneal injection for GTT, and blood sampling was performed to measure blood glucose levels at 0, 30, 60, 90, and 120 min after glucose loading. To determine urinary albumin excretion, individual rats were caged in metabolic cages and 24-h urine samples were collected at 20 weeks of age and at the end of the study. Urinary albumin concentrations were determined by competitive ELISA (Shibayagi, Shibukawa, Japan) and corrected for urinary creatinine concentration. Plasma visfatin concentrations were measured with a visfatin enzyme immunoassay kit (Phoenix Pharmaceuticals, Burlingame, CA, USA) at 20 weeks of age and at the end of the study. Rats were killed under anesthesia by intraperitoneal injection of sodium pentobarbital (50 mg/kg). All experiments were conducted in accordance with the Korea University Guide for Laboratory Animals.

Analysis of gene expression by real-time quantitative PCR in renal tissues and cells

Total RNA was extracted from renal cortical tissues or experimental cells using Trizol reagent and further purified using an RNeasy Mini kit (Qiagen, Valencia, CA, USA). Primers were designed from respective gene sequences using the Primer 3 software, and templates' secondary structures were examined and excluded using the *m*fold software. Table 3 shows the nucleotide sequences of all of the primers used in this study. Quantitative gene expression was performed with a LightCycler 1.5 system (Roche Diagnostics Corporation, Indianapolis, IN, USA) using SYBR Green technology. Real-time reverse transcription-PCR was performed for 10 min at 50 °C and 5 min at 95 °C. Subsequently, 23–30 cycles were applied, which consisted of denaturation for 10 s at 95 °C and annealing with extension for 30 s at 60 °C. At the end of the 30 cycles, samples were heated to 95 °C to verify that a single PCR product was obtained during amplification. The ratio of each gene and β-actin level (relative gene expression number) was calculated by subtracting the threshold cycle number (C_t) of the target gene from that of β-actin and raising 2 to the power of this difference.

Histological examination and immunohistochemical staining for visfatin

Kidney tissues embedded in paraffin were cut into 4-μm-thick slices and stained with periodic acid–Schiff stain. A semi-quantitative score (SI) was used to evaluate the degree of glomerulosclerosis on periodic acid–Schiff-stained sections according to the method described by Ma *et al.*[38] The severity of sclerosis for each glomerulus was graded from 0 to 4+ as follows: 0, no lesion; 1+, sclerosis of <25% of the glomerulus; 2+, 3+, and 4+, sclerosis of 25–50%, >50–75%, and >75% of the glomerulus, respectively. For immunohistochemical staining, renal tissues were sliced into 4-μm sections and after removal of paraffin and dehydration in xylene followed by graded alcohol concentrations, slides were transferred to a 10-mmol/l citrate buffer solution at pH 6.0. The sections were then heated at 80 °C for 10 min to retrieve antigens for visfatin staining, and after washing the slides in water, 3.0% H_2O_2 in methanol was applied for 20 min to block endogenous peroxidase activity, and the slides were then incubated at room temperature for 20 min with normal goat serum to prevent nonspecific detection. Next, slides were incubated for 1 h with primary antibody against rabbit polyclonal anti-visfatin (1:500; Phoenix Pharmaceuticals, Burlingame, CA, USA). The slides were incubated in secondary antibody for 30 min. For coloration, slides were incubated at room temperature with a mixture of 0.05% 3,3′-diaminobenzidine containing 0.01% H_2O_2 and counterstained with Mayer's hematoxylin. Negative control sections were stained under identical conditions except that the buffer solution was used in place of the primary antibody (Supplementary Figure S4). To evaluate the results of immunohistochemical staining, glomerular and tubulointerstitial fields were graded semi-quantitatively by means of grid fields that measured 0.245 mm^2. Briefly, each score was assigned such that it reflected both changes in the extent and intensity of staining. All fields were graded according to a four-point scale, with grade-0 representing absent or <25% of the area positive staining; grade-1, 25–50% of the area positive staining; grade-2, 50–75% of the area positive staining; grade-3, >75% of the area positive staining. More than 50 and 60 glomeruli, and 10 randomly selected tubulointerstitial fields were evaluated under high-power fields ($\times 400$) and average scores were calculated by a pathologist in a masked manner.

Podocytes and PTC culture

A thermosensitive SV 40-transfected immortalized mouse podocyte cell line that was obtained as a generous gift from Peter Mundel at the Albert Einstein College of Medicine (NY, USA) was used for this study. Cultivation of mouse podocytes, which were conditionally immortalized with a temperature-sensitive variant of the SV40 large T-antigen (tsA58) and whose activity could be increased by stimulation with γ-interferon, was performed as described previously.[39] Studies were performed using podocytes at 24–28 passages. MCT cells are a cultured line of PTCs harvested originally from the renal cortex of SJL mice and functionally characterized by Haverty *et al.* (a generous gift from Eric G. Neilson, Vanderbilt University, Nashville, TN, USA).[40] The cells were grown in

Table 3 | Primer sequences for real-time quantitative PCR

Target gene	Primer sequence (5′ to 3′)	Amplicon length (bp)	Number of PCR cycles
Mouse visfatin, forward	TGCCGTGAAAAGAAGACAGA	143	24
Mouse visfatin, reverse	ACTTCTTTGGCCTCCTGGAT		
Mouse GLUT-1, forward	TGCAGTTCGGCTATA ACACC	122	30
Mouse GLUT-1, reverse	ACACCTCCCCCACATACATG		
Mouse MCP-1, forward	CTGGATCGGAACCAAATGAG	95	25
Mouse MCP-1, reverse	CGGGTCAACTTCACATTCAA		
Mouse PAI-1, forward	TCCTCATCCTGCCTAAGTTCTC	365	24
Mouse PAI-1, reverse	GTGCCGCTCTCGTTTACCTC		
Mouse TGFβ1, forward	ATACAGGGCTTTCGATCCAGG	96	28
Mouse TGFβ1, reverse	GTCCAGGCTCCAAATATAGG		
Mouse PCα1(I), forward	TGGTCCCTCTGGAAATGCTGGACC	107	27
Mouse PCα1(I), reverse	CAGGAGAACCAGGAGAACCAGG		
Mouse β-actin, forward	GGACTCCTATGTGGGTGACG	118	23
Mouse β-actin, reverse	CTTCTCCATGTCGTCCCAGT		

Abbreviations: GLUT-1, glucose transporter-1; MCP-1, monocyte chemoattractant peptide-1; PAI-1, plasminogen activator inhibitor-1; PCα1(I), pro-collagen-α1 in type-I collagen; TGFβ1, transforming growth factor-β1.
In this experiment, each sample was run in triplicate and the corresponding non-reverse transcribed mRNA sample was used as negative control. The mRNA level of each sample was normalized to that of β-actin mRNA.

Dulbecco's modified eagles medium supplemented with 10% fetal calf serum as described previously.[40] To evaluate the effect of high glucose and angiotensin II on visfatin synthesis, sub-confluent podocytes and PTCs were serum-starved for 24 h, and the medium was then replaced with media containing 30 mM D-glucose or 100 nM angiotensin II. For the group stimulated with visfatin, different concentrations of visfatin were added to the culture media at final concentrations of 1, 10, and 100 ng/ml. In some wells, cells were pretreated for 30 min with 10 μM of cytochalasin-B, an inhibitor of glucose transporters, before visfatin treatment. All experimental groups were cultured in triplicate and harvested at 48 h for extraction of total RNA and protein.

Measurement of glucose uptake in podocytes and PTCs

Cells were starved in serum-free medium for 16 h and then washed three times with phosphate-buffered saline buffer. Cells were then incubated in 1 ml of Krebs-Ringer phosphate Hepes buffer (136 mM NaCl, 4.7 mM KCl, 1.2 mM $CaCl_2$, 2.5 mM Na_2HPO_4, 10 mM Hepes, and 0.1% (w/v) bovine serum albumin, pH 7.4) for 30 min at 37 °C. The cells were then treated with or without 100 ng/ml of visfatin or 100 nM of insulin and incubated for 15 min at 37 °C. The cells were next incubated with 1 μCi of 2-deoxy-[1–3H]-D-glucose and incubated at the indicated time points, which ranged from 10 to 30 min. To exclude non-carrier-mediated glucose uptake, control wells were pretreated with 10 μM cytochalasin-B for 30 min. In some wells, 10 μM of cytochalasin-B, an inhibitor of glucose transporters, was pretreated for 30 min before initiating visfatin treatment. At the indicated time points, media was collected, cells washed three times with phosphate-buffered saline buffer, and lysed in 0.1 N NaOH for 1 h at room temperature (RT). Total radioactivity from media (R^m) and total cell-associated radioactivity from lysates (R^c) were counted using a liquid scintillation counter. True glucose uptake was calculated as follows: glucose uptake $= [R^{(c)}/(R^{(m)} + R^{(c)})]^{sample} - [R^{(c)}/(R^{(m)} + R^{(c)})]^{cytochalasin\text{-}B}$. Radioactivity was normalized for total protein as quantified by the Bradford method. Next, the dose dependency of visfatin in glucose uptake was determined. As peak glucose uptake occurred at 20 min, cells were treated with different concentrations of visfatin at final concentrations of 1, 10, or 100 ng/ml for 20 min, and glucose uptake was measured as described above. Next, we determined whether pharmacological inhibition of MAPK inhibits visfatin-induced glucose uptake. All MAPK inhibitors were purchased from Calbiochem (EMD chemicals, Darmstadt, Germany). Experimental cells were pretreated with various MAPK inhibitors, including LY294002 (PI3K inhibitor, 1 μM), Akt inhibitor (10 μM), U-0126 (Erk inhibitor, 40 μM), and SB 203580 (p38 MAPK inhibitor, 10 μM) for 30 min before being incubated with visfatin (100 ng/ml) for 30 min.

Determination of insulin signal transduction in podocytes and PTCs

To determine whether the biological effect of visfatin is mediated through the insulin signaling pathway, we checked the tyrosine phosphorylation of the IR and IRS-1 as well as binding of PI3K p85 to IRS-1 in the presence or absence of 100 ng/ml of visfatin in cultured cells. For measurement of tyrosine phosphorylation of the IR and IRS-1, cellular protein extract was analyzed by immunoprecipitation with an antibody to the IR (1:50; Cell Signaling Technology, MA, USA) and IRS-1 (1:50; Cell Signaling Technology, MA, USA), and detected by immunoblotting using an antibody to phosphotyrosine (1:50; Cell Signaling Technology, MA, USA). To determine the binding of p85 to IRS-1, immunoprecipitation was also performed using an antibody to IRS-1 and detected by immunoblotting using an antibody to PI3K p85 (10 μg/ml per 100 μg of cellular protein; Abcam, Cambridge, USA).

Protein extraction, fractionation, and western blot analysis

For studying total cellular lysates, cells were lysed in lysis buffer (150 mM NaCl, 50 mM Tris–HCl, pH 8.0, 1% Triton X-100, 1 mM phenylmethylsulfonylfluoride) and the lysate was boiled for 3 min. For microsomal preparations of cells, whole-cell extracts were prepared by incubating the cells in lysis buffer (20 mM Tris–HCl, 100 mM NaCl, 5 mM $MgCl_2$, 1% NP-40, 0.5% sodium deoxychlolate, 10 mM β-glycerophosphate, 0.1 mM orthovanadate, and protease inhibitors) for 30 min. Cytosol and membrane fractions were prepared using the Qproteom Cell Compartment kit (Qiagen, Valencia, CA, USA) according to the manufacturer's instructions. Protein concentrations were measured by BCA protein assay (Pierce, Rockford, IL, USA). Fifty micrograms of each protein sample was loaded for electrophoresis on a 10% SDS–polyacrylamide gel (Tefco,

Tokyo, Japan) under denaturing conditions. The proteins were transferred onto a polyvinylidene difluoride membrane (Immobilon-P; Millipore, Bedford, MA, USA) for 120 min at 250 mA. After the membrane was blocked by incubating with a blocking solution (Tris-buffered saline containing 150 mM NaCl, 50 mM Tris, 0.05% Tween-20 and 5% non-fat milk, pH 7.5) for 1 h at RT, the membrane was hybridized in blocking buffer overnight at 4 °C with either rabbit polyclonal anti-GLUT-1 antibody (1:500; Abcam, Cambridge, USA); rabbit polyclonal anti-MCP-1 antibody (1:200; Santa Cruz Biotechnology, Santa Cruz, CA, USA); rabbit polyclonal anti-PAI-1 antibody (1:500; Santa Cruz Biotechnology, Santa Cruz, CA, USA); rabbit monoclonal Akt and phospho-specific Akt antibody (1:1000; Cell Signaling Technology, MA, USA); rabbit monoclonal antibody to p38 MAPK, phospho-specific p38 MAPK (1:1000; Cell Signaling Technology, MA, USA); or rabbit monoclonal Erk-1/2, phospho-specific Erk-1/2 antibody (1:2000; Cell Signaling Technology, MA, USA). To confirm equal loading and proper microsomal fractionation of protein, goat polyclonal anti-AIF (apoptosis-inducing factor) antibody (1:200; US Biological, Swampscott, MA, USA) was applied to the membrane in blocking buffer overnight at 4 °C. The filter was then washed four times with TBST and incubated with horseradish peroxidase-conjugated secondary antibody diluted 1:1000 for 60 min at RT. Specific signals were detected by the enhanced chemiluminiscence method (Amersham, Buckinghamshire, UK).

Measurement of secreted visfatin, MCP-1, PAI-1, and collagen in cultured supernatants

Secreted visfatin and total soluble collagen was measured in culture supernatants by using the visfatin enzyme immunoassay kit (Phoenix Pharmaceuticals, Burlingame, CA, USA) and the Sircol soluble collagen assay kit (Biocolor, Belfast, Ireland) according to the manufacturer's instructions. For visfatin measurement, 50 µl of sample was incubated at RT for 2 h with 25 µl of primary antiserum and 25 µl of biotinylated peptide in a secondary-antibody-coated plate. The plates were then washed five times with 300 µl of assay buffer. Next, 100 µl of streptavidin–horseradish peroxidase solution was added and the plates were incubated at RT for 1 h. After washing six times, 100 µl of substrate solution was incubated at RT for 1 h and the reaction was terminated by addition of 2 N HCl. Absorbance was then measured at 450 nm using an ELISA reader. To measure collagen, 1 ml of Sirius red reagent was added to 100 µl of test samples and mixed for 60 min at RT using a mechanical shaker. The collagen–dye complex was precipitated by centrifugation at 14,000 g for 10 min. To release bound dye, 1 ml of alkali reagent (0.5 M NaOH) was added to the precipitate and then absorbance was measured at 540 nm using an ELISA reader. MCP-1 and PAI-1 levels were measured by quantitative sandwich ELISA using a commercial kit (MCP-1, Biosource, Camarillo, CA, USA; PAI-1, American Diagnostica, Stamford, CT, USA), according to the manufacturer's instructions. The supernatant levels of visfatin, MCP-1, PAI-1, and collagen were expressed relative to the total protein concentration under each condition.

Statistical analysis

A non-parametric analysis was used as most of the variables, especially *in vivo* data except kidney/body weight, fasting plasma glucose, and systolic blood pressure, were not normally distributed even after logarithmic transformation. Results are expressed as the mean ± s.e.m. A Kruskall–Wallis test was used for comparison of more than two groups followed by a Mann–Whitney *U*-test for comparison, all of which was performed using a microcomputer-assisted program with SPSS for Windows 10.0 (SPSS, Chicago, IL, USA). Correlations between plasma visfatin levels and biochemical parameters were examined using Spearman's rank correlation test. Values of $P < 0.05$ were considered statistically significant.

DISCLOSURE

All the authors declared no competing interests.

ACKNOWLEDGMENTS

We thank Professor Eric G. Neilson for the generous gift of the mouse MCT cell line, and thank Tokushima Research Institute, Otsuka Pharmaceutical Co. Ltd. for provision of OLETF rats. This work was supported by the Brain Korea 21 project and a Korea University grant.

SUPPLEMENTARY MATERIAL

Figure S1. Dual immunofluorescent staining for megalin and visfatin.
Figure S2. Dose-dependent effect of glucose on visfatin gene expression in experimental cells.
Figure S3. Representative western blot for GLUT-1.
Figure S4. Positive and negative control for visfatin immunohistochemistry.
Supplementary material is linked to the online version of the paper at http://www.nature.com/ki

REFERENCES

1. Amann K, Wanner C, Ritz E. Cross-talk between the kidney and the cardiovascular system. *J Am Soc Nephrol* 2006; **17**: 2112–2119.
2. DuBose Jr TD. American Society of Nephrology Presidential Address 2006: chronic kidney disease as a public health threat—new strategy for a growing problem. *J Am Soc Nephrol* 2007; **18**: 1038–1045.
3. Go AS, Chertow GM, Fan D *et al.* Chronic kidney disease and the risks of death, cardiovascular events, and hospitalization. *N Engl J Med* 2004; **351**: 1296–1305.
4. Foley RN, Murray AM, Li S *et al.* Chronic kidney disease and the risk for cardiovascular disease, renal replacement, and death in the United States Medicare population, 1998 to 1999. *J Am Soc Nephrol* 2005; **16**: 489–495.
5. Lago F, Dieguez C, Gomez-Reino J *et al.* The emerging role of adipokines as mediators of inflammation and immune responses. *Cytokine Growth Factor Rev* 2007; **18**: 313–325.
6. Gualillo O, Gonzalez-Juanatey JR, Lago F. The emerging role of adipokines as mediators of cardiovascular function: physiologic and clinical perspectives. *Trends Cardiovasc Med* 2007; **17**: 275–283.
7. Zhang Y, Proenca R, Maffei M *et al.* Positional cloning of the mouse obese gene and its human homologue. *Nature* 1994; **372**: 425–432.
8. Berndt J, Kloting N, Kralisch S *et al.* Plasma visfatin concentrations and fat depot-specific mRNA expression in humans. *Diabetes* 2005; **54**: 2911–2916.
9. Samal B, Sun Y, Stearns G *et al.* Cloning and characterization of the cDNA encoding a novel human pre-B-cell colony-enhancing factor. *Mol Cell Biol* 1994; **14**: 1431–1437.
10. Jia SH, Li Y, Parodo J *et al.* Pre-B cell colony-enhancing factor inhibits neutrophil apoptosis in experimental inflammation and clinical sepsis. *J Clin Invest* 2004; **113**: 1318–1327.
11. Kralisch S, Klein J, Lossner U *et al.* Interleukin-6 is a negative regulator of visfatin gene expression in 3T3-L1 adipocytes. *Am J Physiol Endocrinol Metab* 2005; **289**: E586–E590.
12. Kralisch S, Klein J, Lossner U *et al.* Hormonal regulation of the novel adipocytokine visfatin in 3T3-L1 adipocytes. *J Endocrinol* 2005; **185**: R1–R8.
13. Verma V, Yao-Borengasser A, Rasouli N *et al.* Human visfatin expression: relationship to insulin sensitivity, intramyocellular lipids, and inflammation. *J Clin Endocrinol Metab* 2007; **92**: 666–672.
14. Dahl TB, Yndestad A, Skjelland M *et al.* Increased expression of visfatin in macrophages of human unstable carotid and coronary atherosclerosis: possible role in inflammation and plaque destabilization. *Circulation* 2007; **115**: 972–980.
15. Axelsson J, Witasp A, Carrero JJ *et al.* Circulating levels of visfatin/pre-B-cell colony-enhancing factor-1 in relation to genotype, GFR, body composition, and survival in patients with CKD. *Am J Kidney Dis* 2007; **49**: 237–244.

16. Takebayashi K, Suetsugu M, Wakabayashi S *et al.* Association between plasma visfatin and vascular endothelial function in patients with type 2 diabetes mellitus. *Metabolism* 2007; **56**: 451–458.
17. Brentano F, Schorr O, Ospelt C *et al.* Pre-B cell colony-enhancing factor/visfatin, a new marker of inflammation in rheumatoid arthritis with proinflammatory and matrix-degrading activities. *Arthritis Rheum* 2007; **56**: 2829–2839.
18. Song HK, Lee MH, Kim BK *et al.* Visfatin: a new player in mesangial cell physiology and diabetic nephropathy. *Am J Physiol Renal Physiol* 2008; **295**: F1485–F1494.
19. Ahima RS, Flier JS. Adipose tissue as an endocrine organ. *Trends Endocrinol Metab* 2000; **11**: 327–332.
20. Beltowski J. Apelin and visfatin: unique 'beneficial' adipokines upregulated in obesity? *Med Sci Monit* 2006; **12**: RA112–RA119.
21. Chen MP, Chung FM, Chang DM *et al.* Elevated plasma level of visfatin/pre-B cell colony-enhancing factor in patients with type 2 diabetes mellitus. *J Clin Endocrinol Metab* 2006; **91**: 295–299.
22. Arner P. Visfatin—a true or false trail to type 2 diabetes mellitus. *J Clin Endocrinol Metab* 2006; **91**: 28–30.
23. Kitani T, Okuno S, Fujisawa H. Growth phase-dependent changes in the subcellular localization of pre-B-cell colony-enhancing factor. *FEBS Lett* 2003; **544**: 74–78.
24. Stephens JM, Vidal-Puig AJ. An update on visfatin/pre-B cell colony-enhancing factor, an ubiquitously expressed, illusive cytokine that is regulated in obesity. *Curr Opin Lipidol* 2006; **17**: 128–131.
25. Garcia JG, Moreno Vinasco L. Genomic insights into acute inflammatory lung injury. *Am J Physiol Lung Cell Mol Physiol* 2006; **291**: L1113–L1117.
26. Oki K, Yamane K, Kamei N *et al.* Circulating visfatin level is correlated with inflammation, but not with insulin resistance. *Clin Endocrinol* 2007; **67**: 796–800.
27. de Boer JF, Bahr MJ, Böker KH *et al.* Plasma levels of PBEF/Nampt/visfatin are decreased in patients with liver cirrhosis. *Am J Physiol Gastrointest Liver Physiol* 2009; **296**: G196–G201.
28. Hammarstedt A, Pihlajamaki J, Rotter Sopasakis V *et al.* Visfatin is an adipokine, but it is not regulated by thiazolidinediones. *J Clin Endocrinol Metab* 2006; **91**: 1181–1184.
29. Chu CH, Lee JK, Wang MC *et al.* Change of visfatin, C-reactive protein concentrations, and insulin sensitivity in patients with hyperthyroidism. *Metabolism* 2008; **57**: 1380–1383.
30. Kawano K, Hirashima T, Mori S *et al.* Spontaneous long-term hyperglycemic rat with diabetic complications. Otsuka Long-Evans Tokushima Fatty (OLETF) strain. *Diabetes* 1992; **41**: 1422–1428.
31. Ayo S, Radnik R, Garoni J *et al.* High glucose causes an increase in extracellular matrix proteins in cultured mesangial cells. *Am J Pathol* 1990; **136**: 1339–1348.
32. Kreisberg JI, Radnik RA, Ayo SH *et al.* High glucose elevates c-fos and c-jun transcripts and proteins in mesangial cells cultures. *Kidney Int* 1994; **46**: 105–112.
33. Haneda M, kikkawa R, Horide N *et al.* Glucose enhances type IV collagen production in cultured mesangial cells. *Diabetologia* 1991; **34**: 198–200.
34. Heilig C, Concepcion L, Riser B *et al.* Overexpression of glucose transporters in rat mesangial cells cultured in a normal glucose milieu mimics diabetic phenotype. *J Clin Invest* 1995; **96**: 1802–1814.
35. Haider DG, Schaller G, Kapoiotis S *et al.* The release of the adipocytokine visfatin is regulated by glucose and insulin. *Diabetologia* 2006; **49**: 1909–1914.
36. Coward RJ, Welsh GI, Yang J *et al.* The human glomerular podocyte is a novel target for insulin action. *Diabetes* 2005; **54**: 3095–3102.
37. Mueckler M. Family of glucose-transporter genes. Implications for glucose homeostasis and diabetes. *Diabetes* 1990; **39**: 6–11.
38. Ma LJ, Nakamura S, Aldigier JC *et al.* Regression of glomerulosclerosis with high-dose angiotensin inhibition is linked to decreased plasminogen activator inhibitor-1. *J Am Soc Nephrol* 2005; **16**: 966–976.
39. Kang YS, Park YG, Kim BK *et al.* Angiotensin II stimulates the synthesis of vascular endothelial growth factor through the p38 mitogen activated protein kinase pathway in cultured mouse podocytes. *J Mol Endocrinol* 2006; **36**: 377–388.
40. Haverty TP, Kelly CJ, Hines WH *et al.* Characterization of a renal tubular epithelial cell line which secretes the autologous target antigen of autoimmune experimental interstitial nephritis. *J Cell Biol* 1988; **107**: 1359–1368.